Light Scattering and Small-Angle X-ray Scattering Studies of an Ionomer Poly(styrene–sodium 2-(acrylamido)-2-methylpropanesulfonate) in Polar Solvents

Jian Wang,[†] Zhulun Wang,[†] Dennis G. Peiffer,[‡] Wendel J. Shuely,[§] and Benjamin Chu*[,†,∥]

Chemistry Department, State University of New York at Stony Brook, Long Island, New York 11794-3400, Department of Materials Science and Engineering, State University of New York at Stony Brook, Long Island, New York 11794-2275, Corporate Research Science Laboratory, Exxon Research and Engineering Company, Clinton Township, Route 22 East, Annandale, New Jersey 08801, and Research Division, Chemical Research, Development, and Engineering Center, Aberdeen Proving Ground, Aberdeen, Maryland 21010-5423

Received June 1, 1990; Revised Manuscript Received July 25, 1990

ABSTRACT: Ionomers with very high levels of sulfonate content, poly(styrene–sodium 2-(acrylamido)-2-methylpropanesulfonate) (poly(St–NaAMPS)), in polar solvents were investigated by using laser light scattering (LLS) and small-angle X-ray scattering (SAXS). The aggregation behavior in the dilute-solution regime could be further confirmed by laser light-scattering measurements of the apparent hydrodynamic radius as a function of temperature and concentration. An ionic peak of this polymer solution, as observed in the SAXS pattern, showed a strong concentration dependence but depended less on the sulfonate content. The SAXS pattern was compared with the core–shell model and the liquidlike structure model. A multifold structure of aggregates in poly(St–NaAMPS) solutions was suggested.

I. Introduction

The solution properties of polymeric materials containing up to 10 mol % of ionic groups, which are usually neutralized by metals, have received considerable attention in recent years. For example, the rheological behavior of flexible long-chain polymers can be significantly altered by introducing a small amount of ionic groups. Solution viscosity studies[1-4] have revealed many unique propeties of dilute and semidilute ionomer solutions. Intra- and intermolecular interactions in solution have been suggested to be responsible for the substantial change in the viscosity of nonaqueous ionomer solutions when compared with that of nonionic parent polymers in solution. As a result of the unique ability to cluster, aggregate, and entangle, a diverse range in the rheological behavior of fluid systems containing such polymer additives[5] is achievable, especially when the effective contour length of the final polymer aggregate is very long. The coexistence of intra- and intermolecular interactions would be expected at any concentration in either polar or nonpolar solvents. Laser light-scattering[6] and small-angle neutron-scattering experiments[7] showed that the aggregation behavior owing to ion–pair interactions was strongly dependent on the quality and the polarity of the solvents. In our recent studies[8,9] of the solution behavior of a *pseudo*ionomer, poly(isobutyl methacrylate–(*tert*-butylamino)ethyl methacrylate), which contains an interacting amino group, the existence of large aggregates even at dilute-solution concentrations could be observed by means of light scattering and of magnetic needle rheometry. It seems timely to investigate the solution property of a model ionomer that contains both positive and negative ionic groups, the latter groups being chemically bound to the chain backbone. In addition, the "ordered" structure of an aqueous solution of ionomers, as characterized by a single broad peak in the SAXS pattern,[10] could be considered as another aggregation feature that we might use to investigate the ionic clustering behavior of such ionomers in solution. The ionic peak might be attributed to intermacroion ordering rather than intramacroion ordering for the following reasons: (a) the peak position depended on polymer concentration; (b) a mixture of two different molecular weight fractions of sodium polyacrylate solutions with the degree of polymerization $P_w = 5000$ and 760 gave a single ionic peak; (c) the Bragg distance corresponding to the peak between 0.03 and 0.09 $Å^{-1}$ was fairly large. However, the question seems to be far from resolved as light-scattering measurements have manifested the formation of quite large ionomer aggregates in solution. These aggregates are composed of a certain number of single polymer molecules and are dispersed randomly at dilute-solution concentrations. Furthermore, an application of the Bragg equation to the ionic peak without long-range periodicity in the structure makes little quantitative sense. Therefore, the origin of the "ordered" structure of ionomers in solution remains an open question.

In exploring the aggregate structure, we directed our attention to the internal inhomogeneity of the aggregate. The poly(St–NaAMPS) can be considered to be made up of random segments that like the solvents and that dislike the solvents. The aggregates, analogous to some micelle formation, have an inhomogeneous structure and are collections of chains, not of ionic groups, as in the bulk state. However, these aggregates are not micelles. If we take the aggregate as a "microgel" particle, the localized inhomogeneous copolymer concentration within the particle is in the semidilute regime. The aggregate is a collection of chains formed mainly by interactions between ionic groups. Thus, ordered packing, if it exists, is possible among the macromolecular chains. SAXS measurements of ionomers in the bulk state showed an ionic diffraction peak that could be interpreted by two different mechanisms. The peak arises from the interference between (1)

* Author to whom all correspondence should be addressed; use Chemistry Department address.
† Chemistry Department, State University of New York at Stony Brook.
‡ Exxon Research and Engineering Company.
§ Aberdeen Proving Ground.
∥ Department of Materials Science and Engineering, State University of New York at Stony Brook.

0024-9297/91/2224-0790$02.50/0 © 1991 American Chemical Society

intermolecular and/or (2) intramolecular ionic aggregates. The ionomer aggregates in the bulk state and that in solution are comparable except for the fact that the aggregates in solution could be swelled (or collapsed) dramatically by solvent and were separated from one another. The combination of light scattering with SAXS permits us to determine the apparent cluster size and its distribution as well as the local structure of the aggregates. The goals were aimed at a better understanding of the ionomer solutions over a variety of environments and of the origin of the SAXS peak in ionomer solutions.

In the present article, we report the results of copolymers of styrene with sodium 2-(acrylamido)-2-methylpropanesulfonate in the presence of a relatively high level of sulfonate content (say, ~60 mol %) in *N*-methylformamide (MFA) or methanol solutions by means of laser light scattering and SAXS. It should be noted that we have used an expanded definition for an ionomer to include polymers containing a high level of ionic content. The SAXS patterns were then analyzed and compared with theoretical models, e.g., the core–shell model[11] and the liquidlike model.[12]

II. Theoretical Background

II.1. Dynamic Light Scattering. The measured photoelectron count autocorrelation function in the self-beating mode has the form

$$G^{(2)}(t,\mathbf{q}) = A(1 + b|g^{(1)}(t,\mathbf{q})|^2) \quad (1)$$

where A is the background (or base line), b is a parameter that accounts for the nonideal point detector, and $g^{(1)}(t,\mathbf{q})$ is the normalized first-order electric field autocorrelation function at delay time t and scattering vector $\mathbf{q}$ ($|\mathbf{q}| = (4\pi n_0/\lambda) \sin(\theta/2)$ where n_0 is the refractive index of the solvent, λ is the wavelength of the incident beam in vacuo, and θ is the scattering angle). For a polydisperse system, $|g^{(1)}(t)|$ is related to the normalized characteristic linewidth distribution function, $G(\Gamma)$, by the relation

$$|g^{(1)}(t)| = \int_0^\infty G(\Gamma)\, e^{-\Gamma t}\, d\Gamma \quad (2)$$

where Γ is the characteristic line width. Laplace inversion of eq 2 could be achieved by using different approaches, such as (i) the cumulants expansion,[13] (ii) the multiexponential singular value decomposition (MSVD) technique,[14,15] (iii) the regularized inversion of the Laplace integral equation,[15] and (iv) the CONTIN method as provided by Provencher.[16,17] From the correlation function profile analysis, an estimate of the polymer hydrodynamic size and its size distribution could be computed. Unfortunately, the Laplace inversion is related to the well-known ill-conditioned problem. So, one should exercise extra care in extracting reasonable information from eq 2. In the present analysis, we were concerned mainly with the cumulants approach in which $|g^{(1)}(t)| = \exp[-\bar{\Gamma}t + (\mu_2/2)t^2 - (\mu_3/3!)t^3 + ...]$, yielding an average line width, $\bar{\Gamma}$, and a variance, $\mu_2/\bar{\Gamma}^2$, with $\bar{\Gamma} = \int \Gamma G(\Gamma)\, d\Gamma$ and $\mu_2/\bar{\Gamma}^2 = \int [(\Gamma - \bar{\Gamma})^2/\bar{\Gamma}^2] G(\Gamma)\, d\Gamma$. By extrapolating $\bar{\Gamma}/q^2$ to zero q, we could determine the Z-average translational diffusion coefficient D_0 ($=\lim_{q\to 0} \bar{\Gamma}/q^2$) at concentration C within the dilute-solution regime. An application of the Stokes–Einstein equation yields an apparent hydrodynamic radius $R_h = k_B T/(6\pi\eta_0 D_0)$ where η_0 is the solvent viscosity and $k_B T$ is the thermal energy.

II.2. Light-Scattering Intensity Measurement. The excess light-scattering intensity of a single particle could be expressed as a product of the interparticle structure factor, $S(q)$, and intramolecular form factor, $F(q)$

$$I(q) \sim S(q)\, F(q) \quad (3)$$

For a hard-sphere particle with radius R, the structure factor that is associated with particle interactions can be represented by the Percus–Yevick (PY) approximation[18]

$$S(q) = 1/[1 - d\tilde{C}(q)] \quad (4)$$

where d is the number density of the particles, $\tilde{C}(q) = 4\pi \int_0^{2R} r^2 C(r)\, [\sin(qr)/qr]\, dr$, $C_{PY}(r) = \alpha + \beta(r/2R) + \gamma(r/2R)^3$ for $0 \le r \le 2R$ and $C_{PY}(r) = 0$ for $r > 2R$. The coefficients α, β, and γ are simple functions of the volume fraction of hard sphere $\phi = (\pi/6)(2R)^3 d$ where $\alpha = -(1 + 2\phi)^2(1 - \phi)^{-4}$, $\beta = 6\phi(1 + \phi/2)^2(1 - \phi)^{-4}$, and $\gamma = -(\phi/2) \times (1 + 2\phi)^2(1 - \phi)^{-4}$. The form factor for the hard sphere has the form

$$F(q) = [\int_v \rho(r) \sin(qr)/(qr)(4\pi r^2)\, dr]^2 \approx [(4\pi/3)R^3 \rho(r)\, \Phi(qR)]^2 \quad (5)$$

where ρ is the electron density distribution and

$$\Phi(qR) = 3[\sin(qR) - (qR)\cos(qR)]/(qR) \quad (6)$$

Considering the fact that there exists a polydispersity with respect to particle size that can be measured by dynamic light scattering, we presume the size distribution could follow a Gaussian distribution. Then, the form factor can be expressed by an integral over all particle sizes

$$F'(q) = \int_0^\infty [(4\pi/3)R^3 \rho(r)\, \Phi(qR)]^2 \exp[-(R - R_0)^2/(2\sigma^2(R))]\, dR \quad (7)$$

where R_0 is the average radius of the particles and σ is the standard deviation with respect to the particle size. The light-scattering intensity curve over the whole range of q for hard-sphere particles is proportional to eq 3 in combination with eqs 4 and 7.

II.3. SAXS. The excess scattered intensity from a sample irradiated by a monochromatic beam of X-rays is given by

$$I(q) = I_e(q)\{\int_v \rho(\mathbf{r})\, e^{-i\mathbf{q}\cdot\mathbf{r}}\, d\mathbf{r}\}^2 \quad (8)$$

where $I_e(q)$ is the scattered intensity by a single electron, $\rho(\mathbf{r})$ is the electron density distribution, and $e^{-i\mathbf{q}\cdot\mathbf{r}}$ is the phase factor. The squaring of the Fourier transform integral over the scattering volume (V) is defined as the multiplication by its complex conjugate. The scattered intensity profile could, in principle, be calculated by using eq 8 for any isotropic microstructure if the particle geometry and the electron density distribution are known. MacKnight et al.[11] proposed a core–shell (CS) model of ionomer morphology in the bulk state on the supposition that the internal structure of each intramolecular ionic aggregate dominates the SAXS peak. A dense core of ionic aggregate is shielded from the surrounding ions primarily by a shell of hydrocarbon chains. At a preferred distance from the core, a shell of ionic materials is attracted to the core through electrostatic interactions. For this model, eq 8 is reduced to

$$I_{CS}(q) = I_e(q)\, N\{4\pi/3[\rho_1 R_1^3 \Phi(qR_1) + \rho_2 R_3^3 \Phi(qR_3) - \rho_2 R_2^3 \Phi(qR_2)]\}^2 \quad (9)$$

where N is the number of particles in scattering volume. Yarusso and Cooper[12] suggested a hard-sphere liquidlike (ll) model by assuming that the aggregates are arranged in space in a liquidlike degree of order with a boundary

Table I
Composition of the Copolymers of Styrene (M_1) with Sodium 2-(Acrylamido)-2-methylpropanesulfonate (M_2)

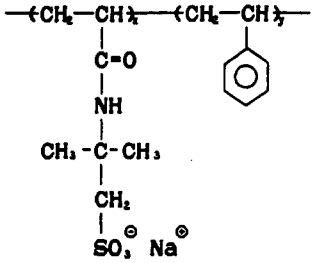

sample	mole ratio M_1:M_2	sulfonate content, mol %
13615-50p	83.5:16.5	16.5
13615-54p	52.9:47.1	47.1
13615-63p	33.3:66.7	66.7

limit of $2R_{CA}$ and $2R_{CA}$ being the distance of closest approach between two aggregates. Physically, it pictures that each aggregate must be coated with an attached layer of hydrocarbon material, which sets up a limitation on the distance of closest approach between two aggregates. The expression is

$$I_{II}(q) = I_e(q)\, NV_1^2\rho^2\Phi^2(qR_1)\frac{1}{1 + 8(V_{CA}/V_p)\epsilon\Phi(2qR_{CA})} \tag{10}$$

where $V_{CA} = (4\pi/3)R_{CA}^3$, $V_1 = (4\pi/3)R_1^3$, ϵ is a constant very close to 1, and V_p is the average volume of the particle. The liquidlike model takes care of interparticle interactions and attributes the SAXS peak to the interference between different ionic aggregates.

III. Experimental Section

III.1. Sample. Copolymers of poly(St–NaAMPS) were prepared by free-radical copolymerization of styrene with sodium 2-(acrylamido)-2-methylpropanesulfonate monomer in dimethylformamide (DMF). The consequent copolymer was precipitated from DMF with hot isopropyl alcohol and dried in a vacuum oven at 25 °C for 24 h. Dietert sulfur analysis was used to determine the sulfonate content and the compositions of NaAMPS. The preparation procedure has been described in more detail elsewhere.[19] The characterization parameters and the structure are listed in Table I.

Solutions were prepared by dissolving the ionomers in redistilled *N*-methylformamide (MFA) and methanol solvents of high grade (purchased from Aldrich Chemical Co.) in optical vials, which can be directly used as sample cells in our magnetic needle rheometer[20] for rheological property measurement at 45 °C for a couple of weeks with occasional shaking by hand. The solutions were then kept at room temperature for another week to enable them to approach equilibrium. The sample solutions were kept in a black box at all times in order to keep the solvent MFA from being decomposed by visible light. For the light-scattering experiments, solutions were clarified carefully by centrifugation for 4 h at 3000–5000 gravity and transferred to dust-free light-scattering cells. Finally, the light-scattering cells were vacuum sealed.

III.2. Light Scattering. A Spectra Physics Model 165 argon ion laser was operated at λ = 488 nm, and an output power of 0.1 W was used as the light source. The sample holder was thermostated to ±0.01 °C over a temperature range from room temperature to ~100 °C. A standard photon counter and a Brookhaven Instruments BI2030 128-channel digital autocorrelator were used to perform light-scattering intensity and time correlation function measurements over an angular range of 15–135°.

III.3. SAXS. SAXS patterns were obtained by using a small-angle X-ray diffractometer equipped with a modified Kratky slit-collimation system[21] and a Braun linear position-sensitive detector at the State University of New York X3A2 Beamline at the National Synchrotron Light Source (NSLS), Brookhaven National Laboratory (BNL). The distance between the sample and the detector was 138 cm, and the resolution of the Braun detector was 0.0093 cm/channel or 0.067 mrad over an angular range of 3 and 35 mrad at λ_0 = 0.154 nm. A sample cell with a thickness of 1.7 mm had two pieces of 25-μm-thick Kapton (Du Pont Co.) films as entrance and exit windows. Polymer solutions could be introduced into the sample chamber (45 × 15 × 1.7 mm) via a top threaded hole, which could be sealed by means of a washer/screw arrangement. The X-ray absorption of polymer solutions studied were around 65% of the incident beam intensity, which is close to the ideal absorption value ($1 - 1/e$). The data acquisition for each sample was carried out over an accumulation time of about 4000 s. The final excess X-ray scattering intensity was corrected for X-ray absorption by the sample, detector intensity and position linearity, incident beam deterioration, and sample thickness. No attempt was made to convert the scattered intensity to absolute scattered intensity.

IV. Results and Discussion

IV.1. Aggregation in Polar Solvent. In the presence of a high degree of sulfonation, poly(St–NaAMPS) would not be expected to be soluble in organic solvents of low dielectric constants but be soluble in polar solvents of high dielectric constants. We started with an extremely polar solvent MFA, whose dielectric constant of 190 is 2.4 times that of water (78.5). By using a membrane osmometer (KNAUER, West Germany), we first tried to determine the molecular weight of our polymer samples. No linear relationship for the reduced osmotic pressure with concentration was observed. The distortion could be attributed to polymer aggregation, which is supposed to occur in nearly all concentrations within the sensitivity of our membrane osmometer. Thus, we failed to determine the molecular weight of single polymer chains and were unable to estimate an apparent number-average molar mass of the polymer aggregate at different dilute concentrations. For the same reason, we did not make any attempt to determine the single-chain dimensions (R_g and R_h) of poly(St–NaAMPS) solution by laser light scattering. Instead, we used laser light scattering, SAXS, and transient electric birefringence (TEB) measurements[22] to study the concentration dependence of apparent dimensions of clusters in dilute and semidilute solution regimes. In spite of the existence of aggregation at all concentrations, we could still treat the aggregates in an ionomer solution as being in the dilute-solution regime so long as the aggregates are isolated from each other. Reduced viscosity measurements can provide us an intuitive insight on the interactions between the particles. Figure 1 shows the reduced viscosity–concentration profiles of poly(St–NaAMPS) solutions in MFA at two different sulfonate contents. Both show typical polyelectrolyte behavior: (1) An upturn at polymer concentrations is revealed below 0.005–0.01 g/mL as is usually observed for polyelectrolytes in aqueous solutions. The upturn could be attributed as due to repulsive forces between fixed ions along the polymer chain. (2) Dilute-solution characteristics are in the concentration range from ~0.01 to 0.04 g/mL, i.e., a flattened curve with a weak and linear concentration dependence. The polyelectrolyte (upturn) behavior for sample 13615-63p (triangles) with 66.7 mol % sulfonation appeared at a lower concentration than that for sample 13615-54p (diamonds) with 47.1 mol % sulfonation. This earlier upturn at a lower concentration for the higher sulfonation content polymer is in reasonable agreement with our expectation that aggregation due to intermolecular interactions occurs at a lower concentration in the case of polymers with more interacting groups.

In checking the existence of association, we employed dynamic light scattering to measure the apparent hydro-

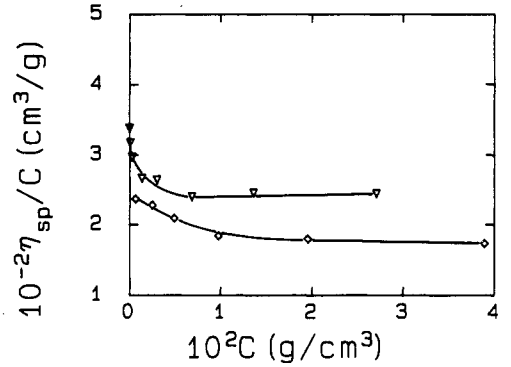

Figure 1. Plots of reduced viscosity against the concentration for ionic copolymer poly(St-NaAMPS) in MFA at 30 ± 0.01 °C. Triangles denote the viscosity behavior of sample 13615-63p with a sulfonate content of 66.7 mol %, and diamonds denote that of sample 13615-54p with a sulfonate content of 47.1 mol %. The measurements at very low concentrations were performed on a capillary viscometer equipped with an optical fiber detector to determine the flow time. Reduced viscosity values at higher concentrations were obtained by means of the magnetic needle rheometer. The two instruments could measure viscosities over a large range of overlapping concentrations and yield consistent results.

Table II
Temperature Effect on Dynamic Light Scattering of Poly(St-NaAMPS) Solution in MFA at $\theta = 45°$

	13615-54p[a]			13615-63p[a]		
	25 °C	55 °C	80 °C	25 °C	55 °C	80 °C
$\bar{\Gamma}$,[b] s^{-2}	164	346	1063	67	124	478
$\bar{\Gamma}/K^2$, 10^{-8} cm^2/s	0.824	1.76	5.51	0.337	0.633	2.48
var[b]	0.34	0.40	0.82	0.33	0.39	0.48
D_o[c], 10^{-8} cm^2/s	0.610	1.63	9.04	0.240	0.600	3.63
R_h[c], nm	216	147	65	551	390	151

[a] 13615-54p, $C = 3.50 \times 10^{-3}$ g/mL; 13615-63p, $C = 4.00 \times 10^{-3}$ g/mL. [b] Data analysis was performed by using a third-order cumulant fit for the correlation functions at 25 and 55 °C and the CONTIN method for those at 80 °C. [c] $D_o = \bar{\Gamma}/q^2(\theta \to 0)$; $R_h = kT/(6\pi\eta_0 D_0)$ in which η_0 changes with temperature.

dynamic size, R_h, in the dilute ionomer solution concentration regime, as shown in Figure 2. The poly(St-NaAMPS) solution in MFA did not give us the usually smooth intensity–intensity time correlation function curves in spite of long accumulation times because of the small value in the refractive index increment (dn/dc). However, temperature has a very strong effect on the correlation function, and the significant difference among these curves permitted us to distinguish them easily. Correlation function profile analysis was performed by using cumulants and CONTIN methods, and the resulting parameters are listed in Table II. It is obvious that after an increase in temperature from 25 to 80 °C, the average characteristic line width, $\bar{\Gamma}$, for each sample is increased substantially. This increase in $\bar{\Gamma}$ could be interpreted in terms of a decrease in the apparent hydrodynamic radius for sample 13615-54p by a factor of 4. We have not extrapolated the measured translational diffusion coefficient (D_0) to infinite dilution because the aggregation behavior is concentration dependent. Thus, the "apparent" R_h includes contributions from intermolecular interactions. However, for qualitative comparisons, it is reasonable to conclude that R_h decreases with increasing temperature. The variation of the variance (Var), which is a measure of the polydispersity of the system in size distribution with temperature, is also evident. Both samples demonstrate larger variance at higher temperatures, implying a broader size distribution at high temperatures. If we associate an improvement in solvent quality with a temperature increase, the

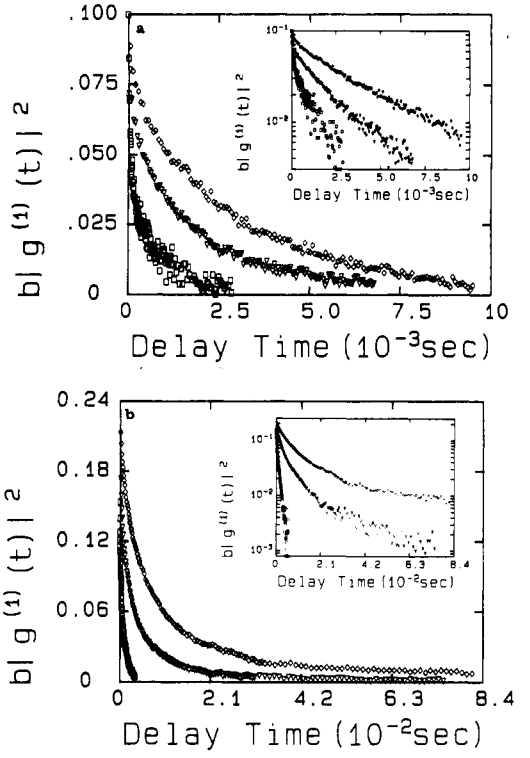

Figure 2. Measured net intensity–intensity time correlation functions of the following ionomers: (a) Sample 13615-54p in MFA at $\theta = 45°$ and concentration $C = 3.50 \times 10^{-3}$ g/mL as a function of temperature. Diamonds denote the curve at 25 °C with delay time increments $\Delta\tau = 70$ μs, triangles, the curve at 55 °C with delay time increments $\Delta\tau = 50$ μs, and squares, the curve at 80 °C with multiple delay time increments $\Delta\tau = 10$, 10, 20, 40 μs. Half-logarithm plots of the time correlation function are shown in the inset following the same symbol meanings. (b) Sample 13615-63p in MFA at $\theta = 45°$ and concentration $C = 4.00 \times 10^{-3}$ g/mL as a function of temperature. Diamonds denote the curve at 25 °C with multiple delay time increments $\Delta\tau = 150$, 300, 600, and 1200 μs, triangles, the curve at 55 °C with multiple delay time increments $\Delta\tau = 140$, 280, 560, and 1120 μs, and squares, the curve at 80 °C with multiple delay time increments $\Delta\tau = 20, 20, 40$, and 80 μs. Half-logarithm plots of time correlation functions in the inset have the same symbol meanings.

decrease in R_h suggests a change in the opposite direction since the polymer chain should be more extended at higher temperatures, implying an increase in R_h rather than a decrease. We interpret the measured decrease in R_h and the increase in Var with temperature as a consequence of partial breaking up of the polymer aggregates. The apparent R_h value for sample 13615-63p is always larger than that for sample 13615-54p at all temperatures in agreement with the reduced viscosity results (see figure 1). In Figure 2 insets the semilogarithm plots show a continuous deviation from the single-exponential behavior. Such tendencies strongly suggest a representation of $G(\Gamma)$ by a unimodal distribution except for those at 80 °C. The unimodal size distribution for polymer aggregates implies that all the polymer molecules have been aggregated over a range of sizes at room temperature. At 80 °C, the aggregates could be broken apart partially, exhibiting broader size distribution and perhaps even nonunimodal behavior. Figure 3 shows the concentration effect on the correlation function of poly(St-NaAMPS) (13615-54p) solution in MFA at $\theta = 25°$ and 25 °C. It is apparent from Figure 3 that the curve at $C = 2.60 \times 10^{-3}$ g/mL (lower concentration) decays faster. The results of curve fitting manifest that the decrease in concentration from 1.00×10^{-2} to 2.60×10^{-3} g/mL brings about a dramatic change in the characteristic line width or in the hydrodynamic

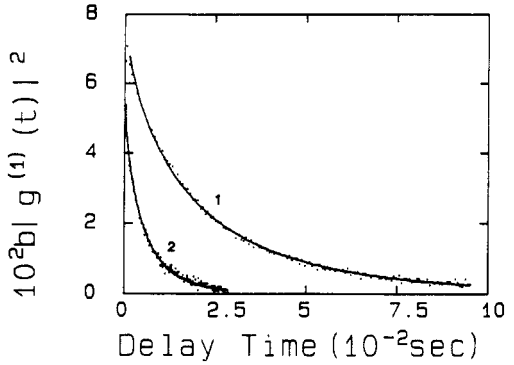

Figure 3. Concentration effect on net intensity–intensity time correlation function of poly(St–NaAMPS) (13615-54P) at θ = 25°, T = 25 °C, and C = 1.00 × 10^{-2} g/mL (curve 1) and C = 2.6 × 10^{-3} g/mL (curve 2). Points denote experimental data, and solid lines are theoretical fitting curves by using the third-order cumulant fit. Curve 1 was taken at $\Delta\tau$ = 700 μs. The fitting parameters are $\bar{\Gamma}$ = 24 s^{-1}; variance = 0.25. By extrapolating q to zero, R_h = 350 nm; curve 2 at $\Delta\tau$ = 59 μs, $\bar{\Gamma}$ = 59 s^{-1}, variance = 0.22. Similarly, from $D_0(q\rightarrow 0)$ we get R_h = 164 nm.

size, which is calculated through extrapolation of $\bar{\Gamma}/q^2$ to q = 0, from R_h = 350 to 164 nm. The apparent hydrodynamic size, R_h, is decreased roughly by a factor of 2.

IV.2. Microstructure of Aggregate. Following the determination of an effective hydrodynamic size and its distribution as a function of temperature and of concentration, SAXS measurements were carried out to investigate the microstructure of polymer aggregates as a function of concentration as illustrated in Figure 4. Great care was taken to treat SAXS data near zero scattering angle because the SAXS pattern in the small scattering angle region could be controversial. We noted that the background parasitic scattering was strong in the small-angle region. In order to reduce the measurement uncertainty, we measured SAXS patterns of the solution, the solvent, and the empty chamber under exactly the same conditions and over the same period of accumulation time. After correction of all scattering curves, the solvent and air backgrounds were subtracted from those of sample solutions. The possibility of an artifact in our SAXS data could be excluded because the observed peak and the small-angle upturn were absent in some polymer samples with lower sulfonate contents where less or no aggregation was anticipated. Figure 4 shows a single broad peak over the concentration range between 0.008 and 0.04 g/mL, and the peak shifts toward larger scattering angles with increasing concentration. The relative intensity of the peak was also enhanced with increasing concentration. Some of the curves did not show an initial small-angle upturn because of the alignment of our SAXS setup, which was optimized to gather the scattered intensity at higher scattering angles. The polymer concentration dependence of the SAXS peak has strengthened our supposition of a short-range ordering of the ionic polymer structure in solution. In Figure 4b, the broad SAXS peak almost disappeared when the concentration was ≤0.004 g/mL. We assert that the small wiggles on the SAXS curves in Figure 4 are experimental noises because of a lack of time in measuring the weak scattering curves, but they clearly showed the existence of a strong (ionic polymer) peak. In some measurements at relatively higher ionomer concentrations, we did have fairly smooth SAXS curves with a single broad peak where no smoothing operation was needed (see for examples curve b in Figure 4a and Figure 5). If the Bragg equation could be applied to the intensity

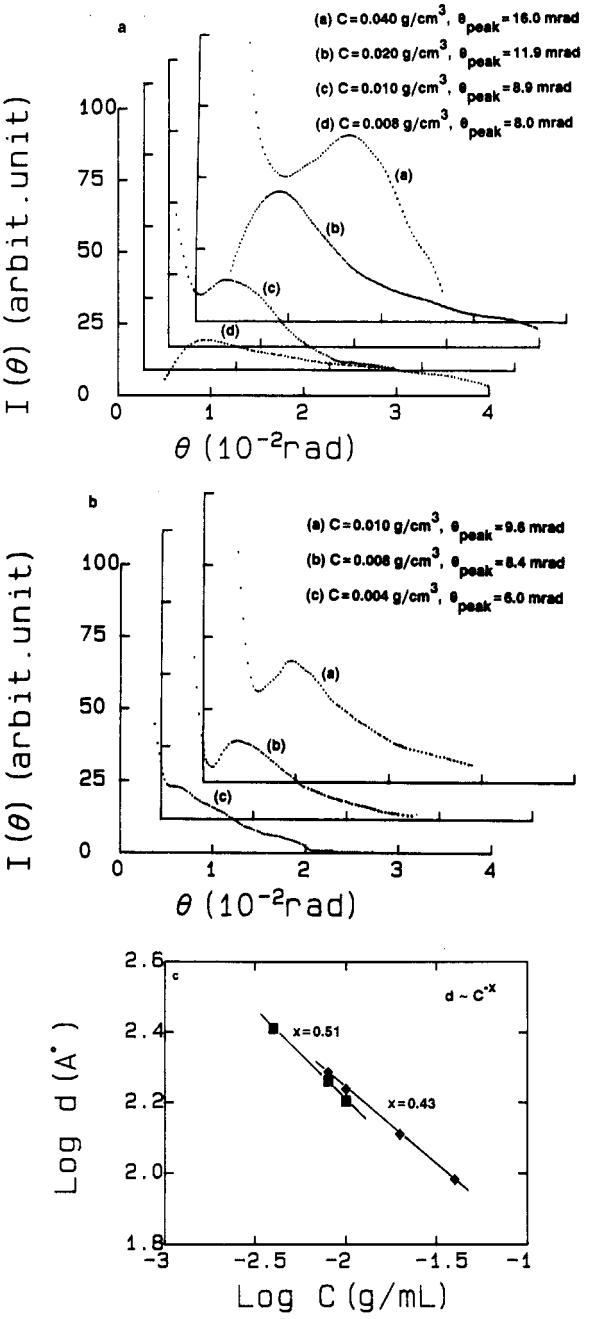

Figure 4. Concentration dependence of excess SAXS intensity of poly(St–NaAMPS) with a sulfonate content 66.7 mol % (a) and with a sulfonate content of 47.1 mol % (b) in *N*-methylformamide at ambient temperatures. Accumulation time = 4000 s for each measurement. The curves presented here were filtered by using a low-frequency-pass filter program in order to minimize the noise level.[23] A strong peak pattern was observed in each curve and the peak position was shifted toward large scattering angles with increasing concentration. (a) and (b) represent two separate sets of experiments. (c) log–log plots of the Bragg spacing versus concentration. Diamonds denote the data in a and squares denote the data in b.

maximum, i.e., the ionic peak, the Bragg spacing for the various samples in Figure 4 would lie between 7 and 26 nm. Figure 4c shows a log–log plot of the Bragg spacing versus concentration, with slopes being 0.43 and 0.51 for the data from parts a and b of Figure 4, respectively. An exponent of 0.43 for the data from Figure 4a is strikingly similar to the Nafion ionomer solution results of Aldebert et al.,[7a] who proposed three different possible structures (a three-dimensional fcc lattice, a hexagonal two-dimensional array of parallel rods, and a cubic phase of rods) and *believed* the results to favor the compact orthogonal

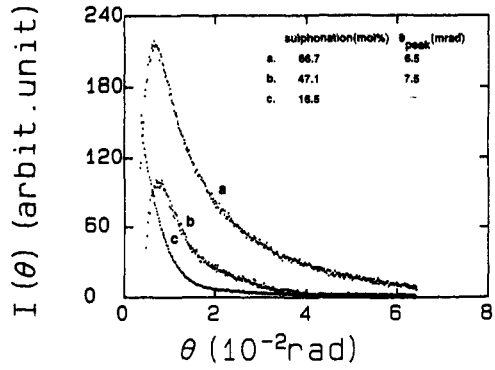

Figure 5. Sulfonate content dependence of excess SAXS intensity of poly(St-NaAMPS) in methanol at $C = 1.00 \times 10^{-2}$ g/mL and ambient temperature with an accumulation time of 3000 s for each measurement. For the polymer sample with the smallest amount of sulfonate content (16.5 mol %), no peak was observed. At 47.1 and 66.7 mol % sulfonate content, only a slight change in the peak position was observed.

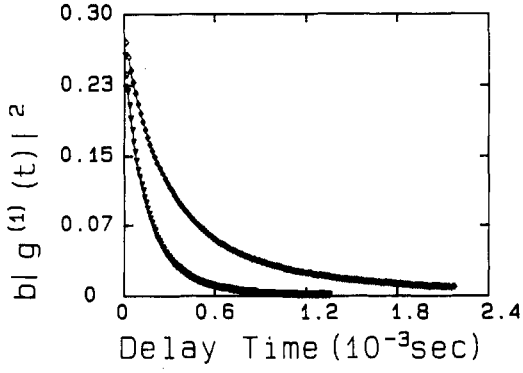

Figure 6. Temperature effect on the intensity–intensity time correlation function of poly(St-NaAMPS) (13615-50p) at θ = 25° and $C = 1.00 \times 10^{-2}$ g/mL in methanol. Hollow diamonds denote the experimental data with delay time increment $\Delta\tau$ = 16 μs at 25 °C, and hollow inverse triangles denote the one with $\Delta\tau$ = 10 μs at 60 °C. Solid lines are the theoretical fitting curves by using the third-order cumulant fit. The fitting results are $\bar{\Gamma} = 1.34 \times 10^2\ s^{-1}$ and Var = 0.31 for the curve at 25 °C and $\bar{\Gamma} = 3.29 \times 10^2 s^{-1}$ and Var = 0.18 for the one at 60 °C. By extrapolation of $\bar{\Gamma}/q^2$ to zero q, we get R_h = 16 nm and R_h = 13 nm for the curves at 25 and 60 °C, respectively.

rod model. The lack of feature in the SAXS pattern clearly makes model fitting difficult. Several different models could fit the experimental data. The SAXS pattern usually cannot determine the uniqueness of the model. The existence of a peak indicates that the electron density inhomogeneities are present in the polymer aggregates over an average distance of ~15 nm, which are not present in monomolecular polymer solutions. The experimental findings of a strong concentration dependence in the position of the ionic polymer peak in solution as shown in Figure 4c could suggest an ordered packing of polymer aggregates in solution. On closer examination, the light-scattering data show polymer aggregates that can diffuse throughout the scattering medium. The polydispersed aggregates do not show an ordered structure in the light-scattering q range. The dimensions of the ionomer peak and its concentration dependence suggest that the ordering must be related to the internal structure of the aggregates. Thus, the SAXS peak must be attributed to the internal structure of the aggregates. The sulfonation effect of poly(St-NaAMPS) in methanol on the ionic peak position is shown in Figure 5. The peak position persisted virtually unchanged after reducing the sulfonate content from 66.7 to 47.1 mol %, but for the sample with 16.5 mol % sulfonate content, the peak was *not* observed. Figure 6 shows the dynamic light-scattering measurement of the sample with 16.5 mol % sulfonate content at θ = 25° and $C = 1.00 \times 10^{-2}$ g/mL in methanol as a function of temperature. In comparison with those samples with higher sulfonate content (see Figure 2), only a weak temperature dependence and a very small aggregate size were observed. The apparent hydrodynamic size calculated by extrapolation of $\bar{\Gamma}/q^2$ to zero q changes from 16 to 13 mm when the temperature is increased from 25 to 60 °C. These observations could suggest a microphase-separation cutoff in connection with the sulfonate content and concentration. The sample with 16.5 mol % sulfonate content probably just falls below the microphase-separation point, resulting in a more homogeneous structure in the polymer aggregates.

IV.3. Interpretation of Microstructure by Models. In this section, we shall explore the microstructure of poly(St-NaAMPS) solution through comparison of experimental data with model calculations. A few models, such as the core–shell model,[11] the liquidlike model,[12] and the depleted-zone core–shell model,[24] have been proposed to explain the ionic peak in the SAXS pattern of ionomers in the *bulk* state. The Debye–Bueche[25] formula has been applied to explain the initial small-angle upturn in the SAXS pattern of ionomers in the bulk state. For ionomer *solutions*, the presence of a large scale in polymer aggregates could not contribute substantially to the scattered intensity in the accessible small-angle q region of our SAXS experiments. There is a difference in the SAXS pattern from the ionomer in the bulk state and that in the solution. For ionomers in the bulk state, we attributed the small-angle upturn to the long-range inhomogeneities mainly due to poor preparation of the polymer melts; i.e., aside from the ionic clusters, the bulk ionomer exhibited long-range inhomogeneities in the ionic distribution throughout space.[26] For ionomer solutions, the disordered polymer is in thermodynamic equilibrium with the solvent and the small-angle upturn, which is not accounted for by the size of the aggregates from light-scattering measurements, represents the inhomogeneities inside the aggregates. An approach to this problem of determining the various scattering intensity contributions could be accomplished as follows. An angular scan of laser light scattering of a poly(St-NaAMPS) solution was made; the light-scattering curve was linked to the SAXS pattern of the same polymer solution; a theoretical light-scattering curve over the whole q range of interest was estimated and then subtracted from the SAXS curve. The subtraction of the theoretical curve due to particle scattering from the SAXS curve would leave us a net SAXS curve resulting only from the microstructures. It should be noted that when the difference is taken in the SAXS pattern between the acid and the salt forms of the same sulfonated polystyrene or between the salt form of the sulfonated polystyrene and the polymer, comparable SAXS patterns due to the ions were obtained.[26] For the same reason, we now assume that the excess SAXS pattern in salt form is equivalent to our excess SAXS pattern between the solution and the solvent, since SAXS by the amorphous polystyrene backbone is comparable to that by the solvent. A hard-sphere model was assumed for the polymer aggregates in an effort to calculate the particle scattering contribution. This model was constructed by multiplication of the structure factor, $S(q)$, with the form factor, $F(q)$ (see eq 3). Figure 7 shows the structure factor of hard spheres as a function of scattering vector, q, with different volume fraction, ϕ, of hard spheres. It is clear that the larger the volume fraction is, the more effect the structure factor has on the scattering pattern. Theoretical

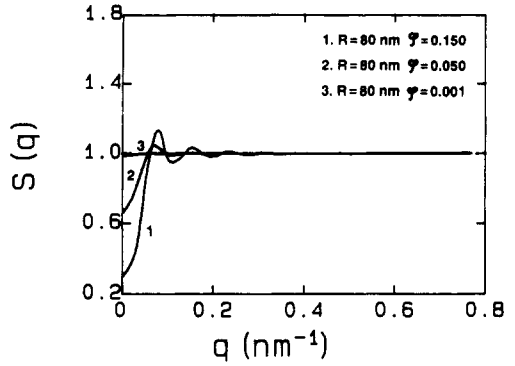

Figure 7. Structure factor of a hard-sphere model as a function of scattering vector q at different levels of the volume fraction of solute particles, calculated by employing eq 4. In the q range of our SAXS experiments (say, 0.15 nm $< q <$ 10 nm), the structure factor is almost unity throughout the scattering angle. On the other hand, in the q range of LLS experiments (say, 0.001 nm $< q <$ 0.03 nm), the structure factor is effective in influencing the excess scattering intensity when the volume fraction of the particles is above 0.1%.

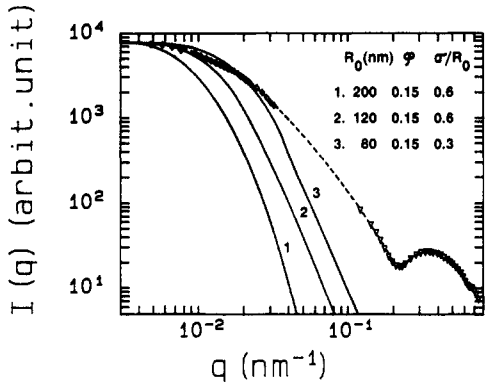

Figure 8. Angular dependence of excess scattering intensity of a dilute solution of poly(St–NaAMPS) in MFA at a concentration of 8.00×10^{-3} g/mL and room temperature. The scattering contributions arising from the entire aggregate in the form of hard spheres are presented as solid curves (eqs 3, 4, and 7). LLS experimental data (diamonds) were linked with SAXS data (triangles) by means of a dashed line, which guides our eyes. With a hard-sphere model for the polymer aggregates the scattering contribution of the large polymer aggregates is small in the q region of SAXS experiments. Subtracting one of the solid curves from the SAXS curve could yield a net SAXS pattern for the internal structure.

curves of hard sphere (solid lines), the measured light scattering (hollow diamonds), and the measured SAXS (inverted hollow triangles) data are linked by the dashed line, as shown in Figure 8. The model parameters in Figure 8 were estimated according to the light-scattering results. The relative deviation, $\sigma(R)/R_0$, with respect to the average size of the hard sphere in a Gaussian distribution could be estimated by the variance of the characteristic linewidth distribution obtained by means of dynamic light scattering. The volume fraction, which has little effect in the q region of our SAXS experiments as shown in Figure 7, was estimated from the concentration and other data, such as the apparent hydrodynamic radius and an estimate of the molar mass of the polymer aggregate, and was fixed at 0.15. The effective hydrodynamic radius of the hard spheres was chosen over a wide range in order to account for the uncertainty in its value. The theoretical calculation based on the hard-sphere model indicates a sharper decrease in intensity with increasing hard-sphere size. Subtracting one of the solid curves from the SAXS pattern seems to be unnecessary here, even for the extreme case of solid curve 3, because of the very small contribution to the scattered intensity in this region by $S(q)$. In linking the light scattering and SAXS curves experimentally, we have assumed a constant shift factor due to refractive index and electron density difference between the two scattering probes. The shift is permissible in a log I versus log q plot. By use of the excess scattered intensity, the effects due to the solvent have been subtracted. In view of the *presence* of metal ions, there is no reason to assume that the two scattering curves over the same q region should be identical. Nevertheless, the main aim for Figure 8 is to illustrate that the finite particle size of the aggregates does not contribute to the SAXS pattern, which measures mainly the internal structure of the aggregates. Figure 9 illustrates some nonlinear regression model-fitting results of our SAXS patterns using the core–shell model and the liquidlike model by means of a Levenberg–Marguardt algorithm. The best fit parameters are listed in Tables III and IV. For the liquidlike model, a very good fit of the ionic peak in each curve could be achieved. However, a deficiency of this model is in the small-angle upturn, which is believed to be indicative of a feature of the polymer aggregates, not long-range inhomogeneities possibly due to poor sample preparations as one would have observed for ionomers in the bulk state. In contrast to the liquidlike model, the core–shell model fits both the small-angle upturn and the ionic peak well and thus seems to be a more reasonable model for poly(St–NaAMPS) in solution. In the core–shell model, the small-angle upturn starts to deviate from the SAXS data from sample 13615-63p, suggesting that the core–shell model cannot quite account for the SAXS pattern of higher sulfonate content poly(St–NaAMPs) ionomers in solution. In any case, a detailed analysis of the SAXS pattern of sulfonated polystyrene suggested that the core–shell model should be modified.[26] Thus, our present analysis is only being used to estimate the ionic cluster size qualitatively. The liquidlike model cannot describe our SAXS patterns. With an additional parameter, the core–shell model can fit the SAXS pattern of poly(St–NaAMPS) including the small-angle upturn for the sample with lower sulfonate content (sample 13615-54p) but not so well at the higher sulfonate content. On the basis of the present SAXS data, the further improvements on the core–shell model are also indicated. Another way to evaluate the ability of a model to predict the SAXS pattern is to compare the electron density–density correlation function of the model with that from experimental data. The present SAXS data do not permit an objective Fourier inversion at this time since the inversion of Fourier transform requires a SAXS curve covering a broader range, preferably from zero scattering angle to the value of q where the intensity falls down to zero. It is also important to check whether the resulting parameters are consistent with what we know about the system. For the core–shell model, the parameters in Table III indicate a reasonable variation according to concentration. When the concentration is decreased, the core radius R_1 and the outside shell radius R_3 are enlarged, while the inside shell radius R_2 remains relatively stable. For the liquidlike model, the parameters in Table IV have a similar tendency. For bulk ionomers, the ionic peak was found[26] in the q region to be about 3-fold larger than that of the peak in our ionomer solution, and the corresponding core–shell model fitting gave rise to a much smaller core or shell size (say, $\sim$1 and $\sim$4 nm in radius for the core and the shell, respectively) than those of our data. Thus, dilution of ionomer with solvent could be viewed as a process of swelling the aggregates, leading to a larger inhomogeneity scale within the aggregates and a partial breaking up of

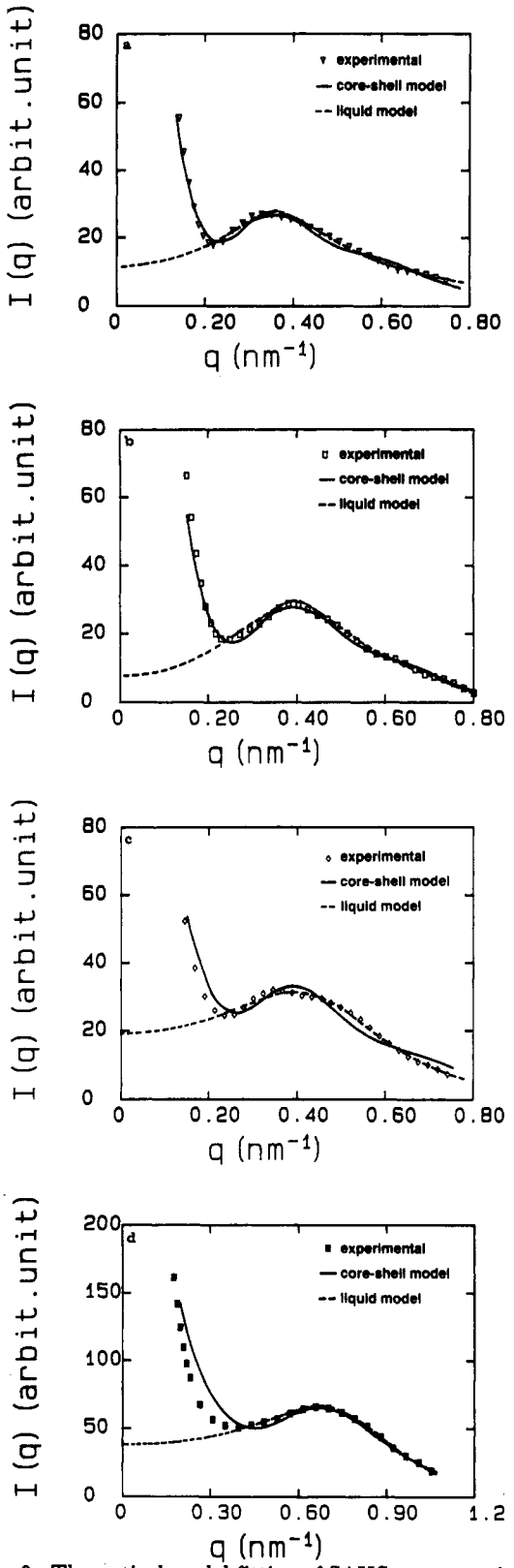

Figure 9. Theoretical model fitting of SAXS patterns of poly(St-NaAMPS) solution in MFA at room temperature by means of a Levenberg–Marquardt algorithm: (a) sample 13615-54p, $C = 8.00 \times 10^{-3}$ g/mL; (b) sample 13615-54p, $C = 1.00 \times 10^{-2}$ g/mL; (c) sample 13615-63p, $C = 1.00 \times 10^{-2}$ g/mL; (d) sample 13615-63p, $C = 4.00 \times 10^{-2}$ g/mL. All model fitting parameters are listed in Tables III and IV.

aggregates. If we forget about the initial small-angle upturn, the liquidlike model would also be applicable. However, the liquidlike model was proposed on the basis of the Zernike–Prins equation,[27] which attributes the scattering peak to an interparticle interference. In the present context, if we accept the small-angle upturn as intrinsic to the microstructure of the aggregates, not inhomogeneities due to solution preparations, a modified core–shell model appears to provide a better description of the SAXS pattern. However, in either case, the aggregates of our ionomer solution possess an average radius of a few hundred nanometers as determined by light scattering, and the central core with its surrounded shell (or hard sphere with its coated layer) is only about 20 nm in radius according to the core–shell model. Thus, in each aggregate there are many (ionic clusters) that are separated by localized hydrocarbon chains and solvents. This "internal structure" of aggregates is responsible for the observed peak in the SAXS pattern. It is not surprising that when an ionomer solution is sufficiently dilute, the ionic peak will disappear in the SAXS pattern.

Table III
Theoretical Fitting Parameters of the Core–Shell Model

sample	concn, g/mL	R_1, nm	R_2 nm	R_3, nm	ρ_1/ρ_2
13615-54p	0.008	3.60	11.1	24.6	194
13615-54p	0.010	2.92	11.5	22.3	354
13615-63p	0.010	3.50	12.6	21.7	203
13615-63p	0.040	2.20	10.0	11.2	53

Table IV
Theoretical Fitting Parameters of the Liquidlike Model

sample	concn, g/mL	R_1 nm	R_{CA}, nm	ρ
13615-54p	0.008	3.34	7.14	0.0362
13615-54p	0.010	2.73	6.55	0.0803
13615-63p	0.010	3.80	5.77	0.0306
13615-63p	0.040	2.84	3.37	0.1230

V. Conclusions

The aggregation behavior of an ionomer poly(St-NaAMPS) in polar solvents was further confirmed by light-scattering and reduced-viscosity measurements. The polymer aggregate formation depended strongly on temperature and concentration. A SAXS peak was observed by using synchrotron SAXS. The peak position depended upon concentration. There was no substantial change in the aggregate microstructure over a range of sulfonate content. The SAXS pattern containing the (ionic) peak could be interpreted in terms of the core–shell model and the liquidlike model. However, the core–shell model provided a better fit if the small-angle upturn were also taken into account. In view of the limited small-angle scattering range that we covered in our SAXS experiments, we do not exclude the possibility of a liquidlike model at this time. According to the core–shell model, the ionic domains are ~3 nm in radius for the center core and ~10 and ~20 nm in inside radius and outside radius, respectively, for the shell. The liquidlike model provides an ionic domain of ~3 nm in radius for the sphere and ~14 nm for the distance of closest approach between the two spheres. A schematic representation of poly(St-NaAMPS) over the concentration range we have studied in polar solvents could be that the formation of large separate polymer aggregates that are randomly distributed can diffuse throughout the fluid. Each aggregate contains core–shell domains that are responsible for the SAXS pattern. The concentration dependence of the ionic peak and of the aggregate dimension could be explained by a solvent swelling of the aggregates in such a way that the ionic domains are also enlarged, while individual aggregates could reduce its degree of association.

Acknowledgment. B.C. gratefully acknowledges support of this research by the U.S. Army Research

Office (DAALO387K0136). The SUNY X-3 beamline is supported by the Department of Energy (DEFG0286ER45321A003) at the National Synchrotron Light Source (NSLS), Brookhaven National Laboratory (BNL).

References and Notes

(1) Lundberg, R. D.; Makowski, H. S. *J. Polym. Sci., Polym. Phys. Ed.* **1980**, *18*, 1821.
(2) Lundberg, R. D.; Phillips, R. R. *J. Polym. Sci., Polym. Phys. Ed.* **1982**, *20*, 1143.
(3) Lundberg, R. D.; Phillips, R. R. *J. Polym. Sci., Polym. Lett. Ed.* **1984**, *22*, 377.
(4) Hara, M.; Win, J. L. *Macromolecules* **1986**, *19*, 2887.
(5) Thaler, W. A.; Walker, T. O.; Lundberg, R. D.; Wagensommer, J. U.S. Patent 4442011, assigned to Exxon Research and Engineering Co., 1984.
(6) Lantman, C. W.; MacKnight, W. J.; Peiffer, D. G.; Sinha, S. K.; Lundberg, R. D. *Macromolecules* **1987**, *20*, 1096.
(7) (a) Aldebert, P.; Dreyfus, B.; Pineri, M. *Macromolecules* **1986**, *19*, 2651. (b) Lantman, C. W.; MacKnight, W. J.; Higgins, J. S.; Peiffer, D. G.; Sinha, S. K.; Lundberg, R. D. *Macromolecules* **1988**, *21*, 1339.
(8) Chu, B.; Wang, J.; Shuely, W. J. *Macromolecules* **1990**, *23*, 2252.
(9) Chu, B.; Wang, J.; Shuely, W. J. *Polymer* **1990**, *31*, 805.
(10) Ise, N.; Okubo, T.; Kunugi, S.; Matsuoka, H.; Yamamoto, K.; Ishii, Y. *J. Chem. Phys.* **1984**, *81*, 3294.
(11) MacKnight, W. J.; Taggart, W. P.; Stein, R. S. *J. Polym. Sci., Polym. Symp.* **1974**, *45*, 113.
(12) Yarusso, D. J.; Cooper, S. L. *Macromolecules* **1983**, *16*, 1871.
(13) Koppel, D. E. *J. Chem. Phys.* **1972**, *57*, 4814.
(14) Chu, B.; Ying, Q.; Wu, C.; Ford, J. R.; Dhadwal, H. S. *Polymer* **1985**, *26*, 1408.
(15) Chu, B.; Ford, J. R.; Dhadwal, H. S. In *Methods Enzymology*; Colowick, S. P., and Kaplan, N. O., Eds.; Academic: Orlando, FL, 1985.
(16) Provencher, S. W. *Biophys. J.* **1976**, *16*, 27; *J. Chem. Phys.* **1976**, *64*, 2772; *Makromol. Chem.* **1979**, *180*, 201.
(17) Version 2, March 1984; Courtesy of S. W. Provencher.
(18) Vrij, A.; Jansen, J. W.; Dhont, J. K. G.; Pathmamanoharam, C.; Kops-Werkhoven, M. M.; Fijnaut, H. M. *Faraday Discuss. Chem. Soc.* **1983**, *76*, 19.
(19) Peiffer, D. G.; Kim, M. W.; Kaladas, J. *Polymer* **1988**, *29*, 716.
(20) Chu, B.; Hilfiker, R. *Rev. Sci. Instrum.* **1989**, *60*, 3047.
(21) Chu, B.; Wu, D.; Wu, C. *Rev. Sci. Instrum.* **1987**, *58*, 1158.
(22) Wang, Z.; Wang, J.; Peiffer, D. G.; Chu, B. *J. Polym. Sci., Polym. Phys. Ed.*
(23) Chu, B.; Xu, R. *Rev. Sci. Instrum.* **1989**, *60*, 910.
(24) Fujimura, M.; Hashimoto, T.; Kawai, H. *Macromolecules* **1982**, *15*, 136.
(25) Debye, P.; Bueche, A. M. *J. Appl. Phys.* **1949**, *20*, 518.
(26) Wu, D. Ph.D. Thesis, State University of New York at Stony Brook, 1989.
(27) Zernike, F.; Prins, J. A. *Z. Phys.* **1927**, *41*, 184.